Simplify your imaging workflows

Make research imaging workflows accessible, traceable, and secure with Athena Software for Core Imaging Facilities.

Thermo Scientific™ Athena Software is a premium imaging data management platform designed for core imaging facilities that support materials science research.

Athena Software ensures traceability of images, metadata, and experimental workflows through an intuitive and collaborative web interface.

Find out more at **thermofisher.com/athena**

ThermoFisher SCIENTIFIC

ADVANCED FUNCTIONAL MATERIALS
www.afm-journal.de

3D Printed Bioelectronic Microwells

*Vassiliki Katseli, Michailia Angelopoulou, and Christos Kokkinos**

The in-house and on-demand fabrication of electrochemical integrated biosensors is a great challenge, especially in the field of modern point-of-care diagnostics. 3D printing technology allows the production of specialized electronic devices adapted to the required conditions, and 3D printed thermoplastic electrodes have shown hopeful achievements mainly in enzymatic bioassays. This work describes a novel configuration of integrated all-3D-printed electrochemical microtitration wells (e-wells) for direct quantum dot-based (QDs) and enzymatic bioassays. The e-wells enable the in situ development of complete bioassays, that is, from sample addition to biomarker detection, without the need for external equipment other than a micropipette and a detector. The bioanalytical capability of the 3D e-wells is demonstrated through the voltammetric bioassay of C-reactive protein employing biotinylated reporter antibody and streptavidin-conjugated CdSe/ZnS QDs. In addition, in order to extend their scope to enzymatic biosensing, e-wells are applied to the amperometric determination of hydrogen peroxide by-products, demonstrating their universal applicability in electrochemical bioassays.

1. Introduction

In current medical diagnostics, sensors have made the detection of specific biomarkers, such as proteins and oligonucleotides, feasible, providing information on diagnosis and treatment. The ideal sensor for healthcare institutions should be fabricated on-demand at the point-of-care and needs to be economically viable. In the quest for ideal biodevices, many research efforts are being conducted and the electrochemical biosensors seem to be the most promising candidates for rapid, simple, reliable, and inexpensive bioassays.[1–4] Additionally, the research field of electrochemical sensors is rapidly evolving via the ongoing application of cutting-edge technologies.[4–7] As the biosensors are crucial to producing bio-information, their manufacture is correspondingly important. The fabrication of electrochemical (bio)sensors is typically carried out through conventional techniques, such as screen-printing and photolithography, which are laborious, multistep processes and require expensive reagents and specific masks. Besides, they are based on human experienced manipulation and accuracy.[8–11] These limitations hinder the innovation and high-throughput in automatic and in-house production of cheap and disposable (bio)sensors, which the modern Industrial Revolution 4.0 requires.

On the other hand, 3D printing technologies can accomplish the fabrication of smart electrochemical diagnostic devices addressing the limitations of conventional approaches.[6,7,12–14] Fused deposition modeling (FDM) is a simple 3D printing approach, which is based on the CAD design of the sensor and its printing from thermoplastic filaments. When the filament is inserted into the 3D printer, it is heated to a semi-molten state and extruded on a platform and through its solidification, the programmed sensor is formed.[15–19] This digital fabrication process offers multiple advantages, such as desktop-sized apparatus, design flexibility, and transferability though e-mail ("e-mailed" sensors), fast prototyping, effortlessness of operation by non-trained handlers, while it produces negligible non-toxic waste. In addition, FDM enables the single-step fabrication of multimaterial sensors using filaments with different properties (e.g., conductive and non-conductive) via multiple extruder 3D printers.[20–23] Therefore, this revolutionary technology allows the on-demand fabrication of integrated sensors, which can be produced within a medical setting, thus meeting the core request for specialized biosensors at the point-of-care.

Nevertheless, only a few reports have appeared in the literature applying 3D printed thermoplastic bioelectrodes produced by FDM to the analysis of biomarkers. More specifically, mainly enzymatic biosensors have been produced by immobilization of enzymes on the surface of 3D printed electrodes for the determination of glucose, amino acid enantiomers, hydrogen peroxide, and catechol, while a 3D printed immunoelectrode has been developed for the label-free detection of a nucleoprotein.[24–28] In all these applications, single 3D printed electrodes are used, and the electrochemical measurements are carried out in "large-volume" electrochemical cells, equipped with external reference (RE) and counter electrodes (CE). Parallel to enzymatic bioassays, the coupling of electrochemical sensors with nanoparticles labels, such as quantum dots (QDs), has been demonstrated as a more attractive route for highly sensitive, stable, and selective bioassays.[4,5,29,30] QDs serve as biobarcodes and signal amplifiers, which are detected by anodic stripping voltammetry (ASV) after their acidic dissolution. The notable sensitivity of ASV-QDs bioassays is achieved by the duplex signal amplification deriving from the synergy of voltammetric preconcentration and the large quantity of metallic

V. Katseli, Dr. M. Angelopoulou, Prof. C. Kokkinos
Laboratory of Analytical Chemistry
Department of Chemistry
National and Kapodistrian University of Athens
Athens 157 71, Greece
E-mail: christok@chem.uoa.gr

The ORCID identification number(s) for the author(s) of this article can be found under https://doi.org/10.1002/adfm.202102459.

DOI: 10.1002/adfm.202102459

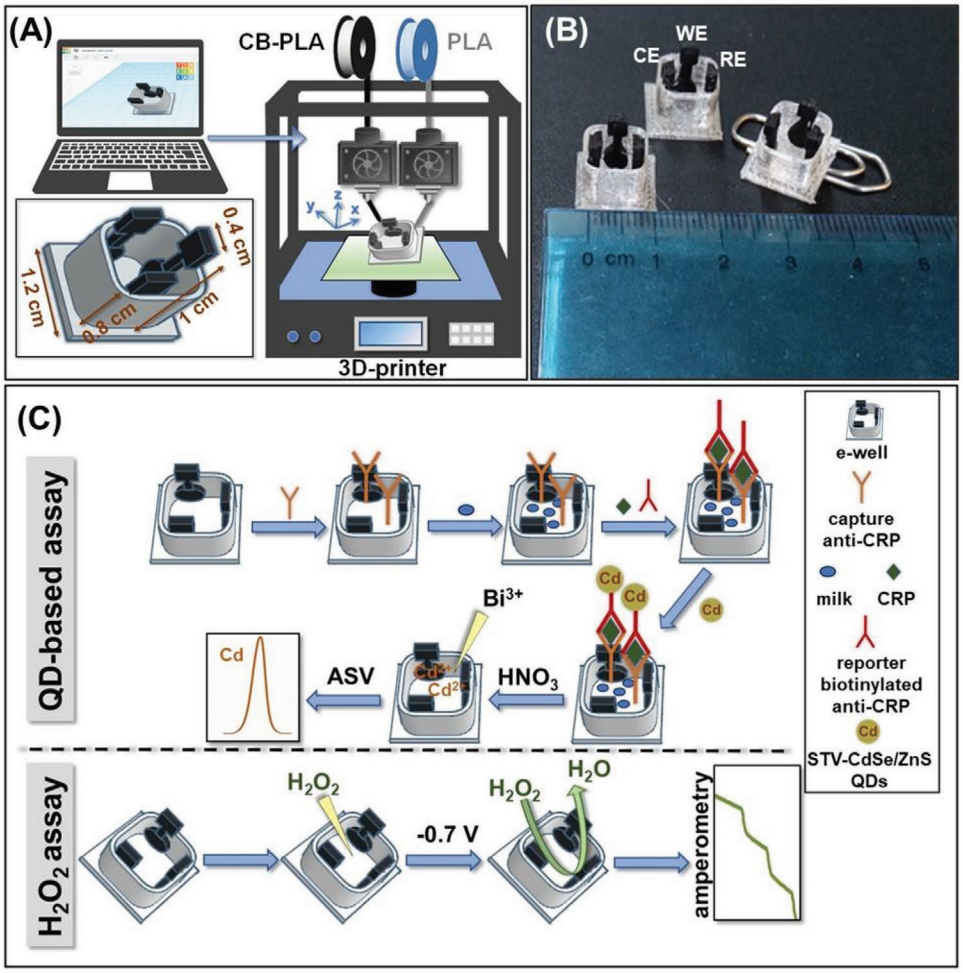

Figure 1. A) 3D printing fabrication procedure of e-well and its dimension in cm. The conductive filament is PLA loaded with carbon black (CB-PLA). B) Photograph of the 3D printed e-wells. C) Schematic illustration of the immunoassay for the QD-based voltametric determination of CRP and for H_2O_2 amperometric assay in 3D e-wells.

cations liberated from QD labels. Despite its great advantages for biosensing, the bioanalytical chemistry arena of 3D printed devices using QDs labels and ASV detection is still unexplored, since no report is published in the pertinent literature.

In this context, we present a new configuration of integrated all-3D-printed electrochemical microtitration wells (e-wells) for micro-volume bioassays (**Figure 1**). The 3D e-wells are fabricated via a single-step printing procedure using a dual extruder 3D printer and are composed of a miniature well (printed from a polylactic acid (PLA) filament) and of three electrodes printed from a carbon-loaded PLA conductive filament integrated on the three sides of each well (Figure 1A,B). The bioanalytical capability of the 3D e-wells to QD-based bioassays is demonstrated through the determination C-reactive protein (CRP) in artificial blood, as this protein is a critical diagnostic biomarker for inflammation, infection, and cardiovascular disease.[31–33] A sandwich-type immunoassay is conducted in the 3D e-well using biotinylated CRP reporter antibody labeled with streptavidin (STV)-conjugated Cd-based QDs. The quantification of the target protein is performed at the 3D e-well after the acidic dissolution of the QDs and ASV determination of the Cd(II) released (Figure 1C). In order to enhance the sensitivity, a bismuth film is deposited on the working electrode (WE) of e-well via an in situ electroplating process. Additionally, as the e-wells are not intended only for QDs-ASV bioassays, their analytical capability is further extended to the amperometric detection of H_2O_2 (Figure 1C). Hydrogen peroxide is the by-product of numerous enzymatic reactions and its measurement is used for the determination of significant biomarkers, such as glucose, lactate, cholesterol, and others.[26,34] In the case of H_2O_2 determination, the e-wells are used as-printed, without any modification with nanoparticles or enzymes.

2. Results and Discussion

2.1. Fabrication and Operational Features of the 3D Printed e-Well

The motivation for the application of FDM printing approach to the production of e-wells is the provision of fabrication simplicity, rapidity, portability, reduction of the manufacture cost and the potential for miniaturization, integration, and array-production. The 3D e-well has the specific mini shape in order

to be adjustable to the necessities of common microtitration well-based bioassays, which usually involve working volumes of about 100 µL. Additionally, the 3D e-well can be designed and printed in arrays of eight or more e-wells. The presented 3D e-well qualifies as lab-on-a-well, since it fulfills the requirement to conduct whole bioassay from sample addition to biomarker detection, without the demand for extra equipment other than a portable potentiostat. Hence, in contrast to common microtitration-based bioassays, the requirement for the transfer of the sample from microwells to separate "large-volume" electrochemical cells is avoided and, thus, the bioassay workflow is simplified and the sample dilution is minimized.

Since commercial available STV-conjugated CdSe/ZnS QDs are preferred as biotags in numerous electrochemical bioassays, the parameters which affect the 3D e-well sensitivity toward the voltametric determination of Cd(II) was initially studied, as Cd(II) released after the acidic dissolution of QDs. Due to the low ASV determination sensitivity of heavy metals at bare carbon-based electrodes, the WE of 3D e-wells was subjected to modification with bismuth and antimony films.[35,36] For this purpose, an in situ electroplating protocol was followed, in which Bi(III) or Sb(III) were added directly into the sample solution and the respective film was deposited on the surface of WE during the preconcentration step and simultaneously with the deposition of Cd on it. As depicted in **Figure 2**A, the comparative voltammograms obtained at the bare carbon-loaded PLA WE and at Bi- and Sb-film carbon-loaded PLA WEs, reveal that the ASV sensitivity of Cd(II) detection at the Bi-film electrode is about 5 and 2.5 times higher than at 3D bare carbon-loaded PLA and 3D Sb-film electrodes, respectively. Thus, bismuth was selected as optimum material for the generation of the metallic film on the surface of the 3D printed WE of e-well. The added Bi(III) concentration used for producing the Bi-film is a key parameter, which affects the electrochemical performance of the e-well toward Cd response. As shown in Figure 2B, in the absence of Bi(III) a small peak of Cd(II) was obtained, suggesting the slightly poor preconcentration of Cd on the bare carbon-loaded PLA. With the presence of Bi(III) in the working solution, higher Cd peaks appeared, and as the Bi(III) concentration increases, the Cd peak heights became larger. Bismuth films generated by electrodeposition of 0.2 and 0.5 mg L^{-1} Bi(III) presented the higher peak currents of Cd, and for the rest of the experiments 0.2 mg L^{-1} Bi(III) was selected, since this concentration offered satisfactory sensitivity in conjunction with lower consumption of the bismuth reagent.

The filament used for the printing of the WE is another critical parameter affecting the electrochemical determination sensitivity. Two different carbon-loaded conductive filaments (PLA and acrylonitrile butadiene styrene (ABS)) were tested, in terms of the square wave ASV (SWASV) peak heights of Cd and of the amperometric responses of H_2O_2. As depicted in Figure 2 (panels C, D) the carbon-loaded PLA filament presented higher stripping peak of Cd with lower background characteristics and significant higher amperometric responses of H_2O_2. Thus,

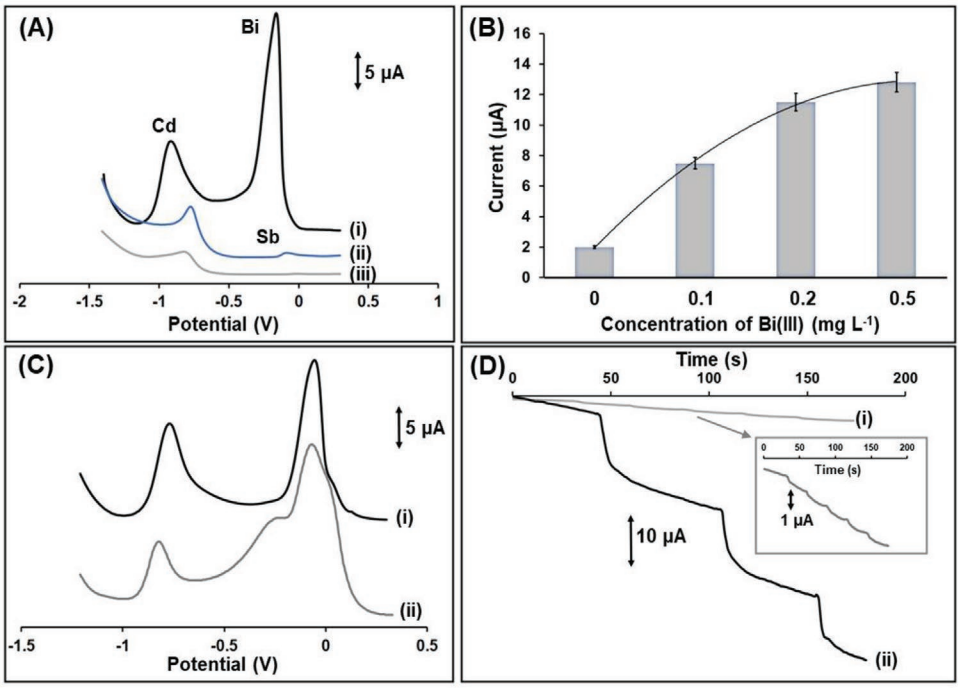

Figure 2. A) Comparative SW voltammograms of 30 µg L^{-1} Cd(II) at 3D printed e-wells with: i) Bi-film modified carbon-loaded PLA WE (electrodeposition with 0.2 mg L^{-1} Bi(III)), ii) Sb-film carbon-loaded PLA WE (electrodeposition with 0.2 mg L^{-1} Sb(III)), and iii) as-printed carbon-loaded PLA WE. B) Effect of the Bi(III) plating concentration on the striping peak height of 30 µg L^{-1} Cd(II). C) SWASV responses of 30 µg L^{-1} Cd(II) at 3D printed e-wells using carbon-loaded WEs printed by: i) PLA (black line) and ii) ABS (gray line). The surface of each WE was covered with a Bi-film in situ formed by electrodeposition with 0.2 mg L^{-1} Bi(III). For (A–C) the supporting electrolyte was HNO_3 0.01 mol L^{-1} and the preconcentration step was for 240 s at –1.4V. D) Amperometric responses of successive additions of 4.5 mmol H_2O_2 in PBS 0.1 mol L^{-1} (pH 7.0) at as-printed e-wells using carbon-loaded WEs from: i) ABS (gray line) and ii) PLA (black line).

carbon-loaded PLA filament was selected for the printing of the WE, as well as for the printing of the CE and RE for reasons of manufacturing simplicity and speed. The differences in electroanalytic characteristics between carbon-loaded PLA and ABS filaments can be attributed to their different amount of the carbon-black content, which affects their resistivity (15 and 0.1 Ω·cm resistivity for carbon-loaded filaments of PLA and ABS, respectively).

The 3D printed PLA WE modified with Bi-film was characterized by optical microscopy. An optical micrograph is illustrated in **Figure 3**A, which shows the surface morphology of bare carbon-loaded PLA WE and after electrodeposition with 0.2 mg L^{-1} Bi(III) at –1.4 V for 240 s and suggests that almost complete coverage of the surface with Bi was succeed. Calibration for Cd(II) using ASV and Bi-film 3D e-well was conducted in the concentration range 10–90 μg L^{-1} (steps of 10 μg L^{-1}) and the respective SWASV voltammograms and the calibration plot are presented in Figure 3B. The e-well exhibited linear concentration dependence in the examined concentration range for Cd(II) with a correlation coefficient (r^2) of 0.997. The limit of detection (LOD) (calculated using the equation LOD = 3sy/a, where sy is the standard deviation of the y residual of the calibration plot and a the slope of the linear calibration curve) was 0.22 μg L^{-1}. These results demonstrate the suitability of 3D e-wells for the ASV determination of cadmium and by extension in bioassays employing Cd-based QDs labeling.

On the other hand, in order to examine the suitability of e-well to H_2O_2 determination, linear sweep (LS) was conducted in 0.1 mol L^{-1} PBS (pH = 7.0) in as-printed 3D e-wells. LS voltammograms in absence and presence of H_2O_2 are presented in Figure 3C. In the absence of H_2O_2 the reduction of hydroxonium anions of electrolyte started at about –1.0 V, while in the presence of 2.5 mmol L^{-1} H_2O_2 the electro-reduction of H_2O_2 started at about –0.7 V, confirming the ability of e-well toward H_2O_2 amperometric determination.

Another significant operational feature of the e-well is both the potential stability and the within-electrode potential reproducibility of the integrated 3D printed carbon pseudo-RE. The potential stability of the 3D printed RE was tested for 20 repetitive measurements, while the within-RE potential reproducibility was evaluated by comparing the results obtained by 6 different 3D printed REs. All comparative measurements were carried out in a solution containing 40 μg L^{-1} Cd(II) in 0.01 mol L^{-1} HNO_3 with 0.2 mg L^{-1} Bi(III). The potential, where the Cd peak appears, remained statistically constant during the 20 repetitive measurements, while the % relative standard deviation (% RSD) of the peak potential of Cd(II) at the 6 different 3D printed REs was 3.2%, indicating satisfactory potential stability and reproducibility.

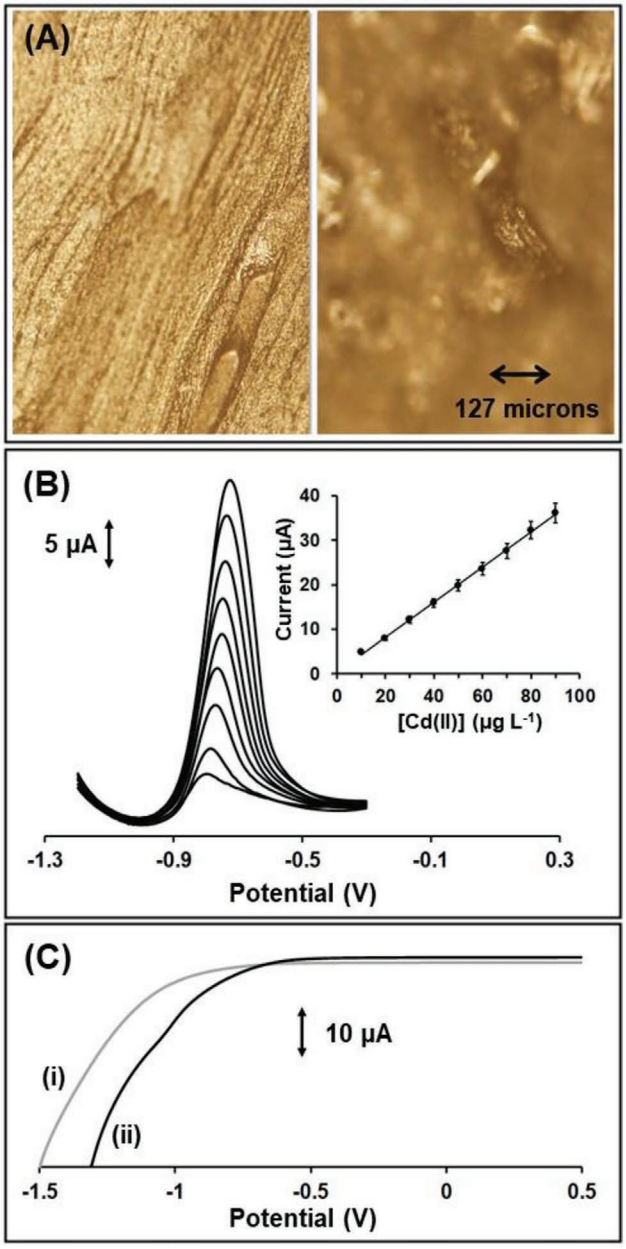

Figure 3. A) Optical micrograph of the 3D printed WE surface before (left) and after (right) electrodeposition of 0.2 mg L^{-1} Bi(III) at –1.4 V for 240 s. B) SW voltammograms for increasing concentrations of Cd(II) in the range 10–90 μg L^{-1} (steps of 10 μg L^{-1}) at 3D printed e-wells modified with Bi-film and (inset graph) the respective calibration plot. The points in the plot are the mean value ± SD (n = 3). C) LS voltammograms of the 3D e-wells in i) 0.1 mol L^{-1} PBS (pH = 7.0) (grey line) and ii) a solution containing 2.5 mmol L^{-1} H_2O_2 (black line). Scan rate, 50 mV s^{-1}.

2.2. Optimization of QD-Based Bioassay and of Hydrogen Peroxide Assay in 3D Printed e-Well

The determination of CRP was performed via a sandwich configuration, involving overnight physisorption of polyclonal anti-CRP antibody in the 3D e-wells, blocking for 1 h, addition of a 1:1 mixture of CRP with biotinylated anti-CRP antibody and incubation for 45 min, and then, reaction with STV-conjugated CdSe/ZnS QDs for 15 min. Next, 150 μL of a solution containing HNO_3 0.01 mol L^{-1} and 0.2 mg L^{-1} Bi(III) were added in each e-well for the SWASV measurements (Figure 1C). Different parameters of the immunoassay were evaluated. Initially, the composition of the assay and washing buffers was investigated testing 10 mmol L^{-1} PBS (pH 7.4), 50 mmol L^{-1} PBS (pH 7.4), Tris-HCl with pH 7.8, and pH 8.2 containing bovine serum albumin (BSA) from 0.5 to 2% w/v. The higher sensitivity in

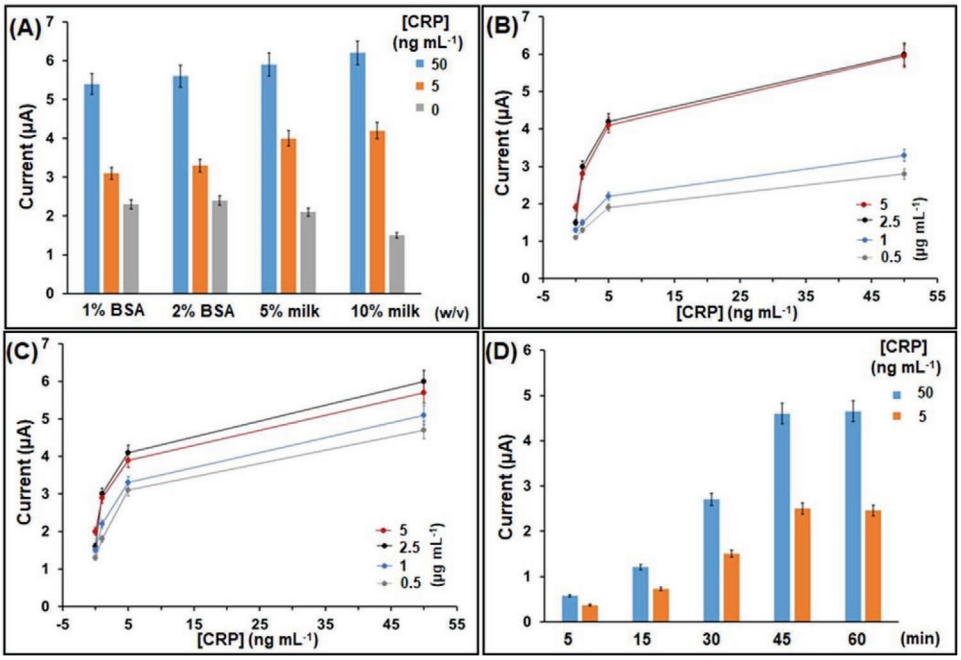

Figure 4. A) Mean current values of CRP calibrators and non-specific signal at 3D e-wells using different blocking solutions. B) Mean current values of CRP calibrators versus the concentration of the capture anti-CRP antibody. C) Mean current values of CRP calibrators with respect to the concentration of the reported biotinylated anti-CRP antibody. D) Effect of the immunoreaction time on the net current values of 5 and 50 ng mL^{-1} CRP. Each point is mean value ±SD ($n = 3$).

conjunction with the lower non-specific binding was achieved when 50 mmol L^{-1} PBS (pH 7.4) containing 1% w/v BSA was used as assay and washing buffer. Next, the composition of blocking solution was tested applying 1 and 2% w/v BSA in 0.1 mol L^{-1} $NaHCO_3$, 5 and 10% w/v skimmed cow milk in 50 mmol L^{-1} PBS (pH 7.4). As shown in **Figure 4**A, 10% w/v cow milk presented the lowest non-specific signal and high responses of CRP and thus, it was chosen as blocking solution. Besides, the concentration of capture anti-CRP antibody in 50 mmol L^{-1} carbonate buffer (pH 9.2) was tested in the range from 0.5 to 5 μg mL^{-1}, using four concentrations of 0, 1, 5, and 50 ng mL^{-1} CRP, 2.5 μg mL^{-1} biotinylated anti-CRP antibody, and 5 nmol L^{-1} QDs. As indicated in Figure 4B, high signals were achieved via coating with 2.5 and 5 μg mL^{-1}, whereas the non-specific binding signal obtained from 2.5 μg mL^{-1} was lower than that of 5 μg mL^{-1} and thus, 2.5 μg mL^{-1} of capture antibody was selected for the assay. Additionally, the concentration of the biotinylated antibody was studied in the range from 0.5 to 5 μg mL^{-1}, and 2.5 μg mL^{-1} offered high signals with low non-specific binding contribution (Figure 4C). The duration of immunoreaction and reaction with the STV-conjugated QDs was also studied. As shown in Figure 4D maximum responses were reached after 45 min of immunoreaction, which were almost equals to those after 60 min. Regarding the reaction with STV-conjugated QDs, a 15 min reaction time provided satisfactory signals, setting a total assay duration just of 1 h. Finally, the effect of the preconcentration time (in the range 60–600 s) and potential (in the range from –1.6 to –0.7 V) was examined using a solution of 10 ng mL^{-1} CRP. A preconcentration step at –1.4 V for 240 s was chosen providing high sensitivity and short measurement procedure.

To improve the sensitivity of the as-printed e-wells to H_2O_2 determination, the pH of solution and the applied potential were studied in an amperometric mode. The effect of pH values on the response of 6 mmol L^{-1} H_2O_2 was tested in pH values ranging from 5.5 to 8.5. By increasing the pH value, the amperometric response of H_2O_2 increased and reached a maximum value at pH 7.0, which was chosen for the assay. Also, the applied potential affects the efficiency of the e-well to H_2O_2 electroreduction and this effect was studied from –0.7 to –0.3 V. The amperometric response of 6 mmol L^{-1} H_2O_2 increased with increasing the negative potential values, and –0.7 V was selected for H_2O_2 measuring at as-printed e-well.

2.3. Analytical Evaluation of the 3D Printed e-Well

The LOD, the dynamic concentration range, the within-well, and the between-well reproducibility were determined under selected experimental parameters. **Figure 5**A shows SWASV voltammograms obtained for different CRP concentrations (0–50 ng mL^{-1}, from bottom to top). The peak current of released Cd(II) of QDs labels was linearly related to the logarithm of the concentration of CRP with $r^2 = 0.996$. The LOD was 0.06 ng mL^{-1} and it considered as the concentration of CRP corresponding to three times the standard deviation of the peak current due to non-specific absorption. This LOD is comparable or lower with that of other electrochemical CRP assays and it is much lower than the minimal clinical level for the estimation of myocardial infarction. Thus, this LOD offers a great practical benefit, as it permits extensive sample dilution minimizing the intense matrix effects of clinical samples.[31–33] Figure 5B

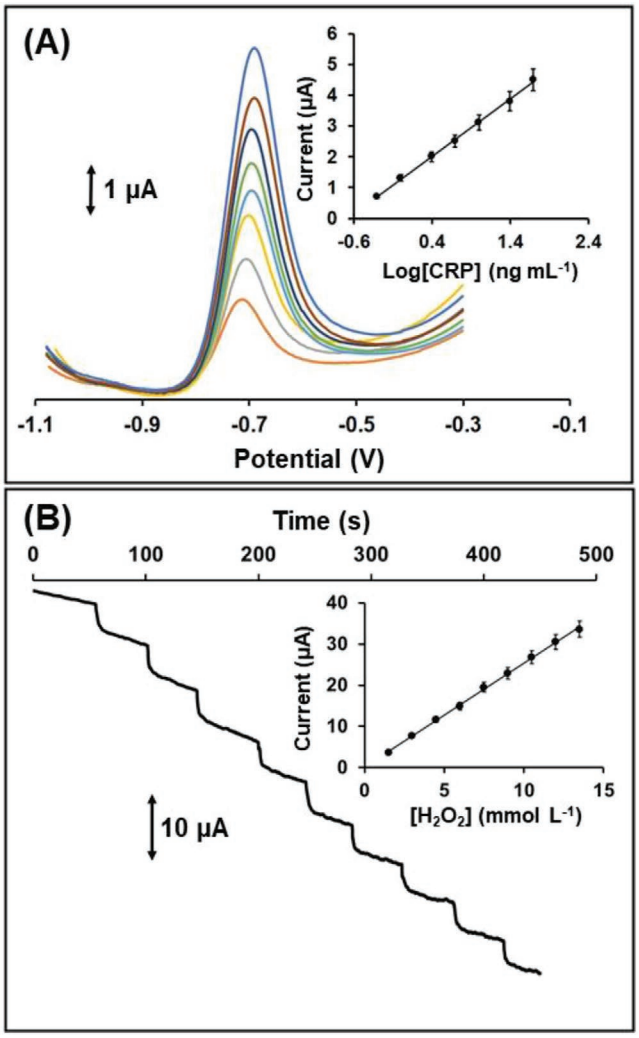

Figure 5. A) SW voltammograms for 0.0, 0.5, 1.0, 2.5, 5.0, 10.0, 25.0, and 50.0 ng mL^{-1} CRP and the respective calibration curve plotted on a semilog scale. Each point in the calibration plot represents the mean value ± SD ($n = 3$) after subtraction of the mean signal corresponding to non-specific absorption. B) Amperometric responses and the calibration plot for H_2O_2 in the concentration range 1.5–13.5 mmol L^{-1}. The points in the calibration plot are the mean value ± SD ($n = 3$).

illustrates the amperometric responses for successive additions of H_2O_2 in 3D e-well and the respective calibration plot (r^2 = 0.999) in the concentration range of 1.5–13.5 mmol L^{-1}. In the case of H_2O_2 determination, the e-wells were used as-printed, without any modification of WE with nanoparticles or enzyme for enhanced sensitivity. Still, the linear range of H_2O_2 determination at 3D e-wells compares well with that of other modified electrochemical sensors.[37–39]

The between-well reproducibility expressed as % RSD using 8 different e-wells was lower than 10.7% over the whole calibration range for CRP analysis and lower than 6.4% for H_2O_2, and the within-well reproducibility (determined as the % RSD of 10 repetitive measurements of a solution containing 40 μg L^{-1} Cd(II) or 6 mmol L^{-1} H_2O_2 at the same e-well) was 4.2% and 3.4% respectively. These values show the satisfactory precision accomplished by the e-wells and justify their suitability for routine analysis.

The accuracy of the CRP QD-based immunoassay was further evaluated through recovery experiments in blood samples. For this purpose, artificial blood samples spiked with 5, 15, and 35 ng mL^{-1} CRP were analyzed. The CRP concentration in the spiked blood samples was estimated through the calibration curve of Figure 5A and the recovery values ranged from 95% to 103%, confirming the accuracy of the CRP e-well assay.

3. Conclusion

For the first time, all-3D-printed e-wells have been fabricated for the direct development of bioassays. As a proof-of-concept, the e-wells were biofunctionalized with specific antibody and used for the sensing of CRP. For this goal, a microliter sandwich-type immunoassay was developed into the 3D e-wells employing Cd-based QDs as labels, while the SWASV determination of the released Cd(II) was carried out at an electrodeposited Bi-film on the surface of integrated WE of e-wells. Additionally, as-printed e-wells were applied to the amperommetric determination of H_2O_2, which is the by-product of several enzymatic assays. In contrast to common microtitration well-based electrochemical bioassays and to the existing single 3D-printed bioelectrodes, the necessity for the transfer of the sample from microwells or of the bioelectrode to separate electrochemical cells is avoided and, thus, the assay workflow is simplified and the sample dilution is eliminated. This work paves the way toward the in-house production of cheap, integrated, specialized, and electrochemical biodevices, covering the demand for sensitive clinical analysis at the point-of-care.

4. Experimental Section

Chemicals and Apparatus: CRP (Human fluids, >99%) and goat polyclonal anti-CRP were from Scripps Laboratories. Monoclonal anti-CRP was from Medix Biochemica. BSA was from Sigma Aldrich. The biotinylation of goat monoclonal anti-CRP was performed according to the literature.[31] STV-conjugated CdSe/ZnS QDs (1 μmol L^{-1}) were from Life Technologies. Aqueous stock Cd(II), Bi(III), Sb(III) solutions were prepared from 1000 mg L^{-1} atomic absorption standard solutions. All the other chemicals were from Merck. The artificial blood was composed of NaCl 116 mmol L^{-1}, $CaCl_2$ 1.8 mmol L^{-1}, KCl 5.4 mmol L^{-1}, $MgCl_2$ 0.5 mmol L^{-1}, $NaHCO_3$ 26 mmol L^{-1}, Na_2HPO_4 0.9 mmol L^{-1}, and NaH_2PO_4 0.2 mmol L^{-1}.[40]

An optical microscope (Karl Suss PA200, SUSS Microtec) was used for the imaging of the surface of the 3D printed WE. Electrochemical experiments were conducted with a PGSTAT101 potentiostat (Metrohm Autolab) operated by NOVA 1.8 software (Metrohm Autolab).

Printing of the 3D e-Wells: The e-wells were designed with Tinkercad software and printed by a dual extruder 3D printer (Creator Pro from Flashforge). The non-conductive filament was transparent PLA from 3DEdge and the conductive filaments were carbon-loaded with PLA and carbon-loaded with ABS obtained from Proto-Pasta and 3DEdge, respectively. The printing conditions were set to 60 °C for the platform, 200 and 220 °C for the head dispensers for PLA and ABS, respectively. The integrated electrodes of the e-well protrude sufficiently from the top of the well for easy connection of the 3D-printed electrodes to the potentiostat via crocodile clips.

Procedures: The construction of the calibration plot of Cd(II) was conducted in the same 3D e-well by adding 100 µL of a solution containing HNO_3 0.01 mol L^{-1} and 0.2 mg L^{-1} Bi(III), followed by nine successive additions of 1 µL of 1 mg L^{-1} Cd(II), under shaking. The preconcertation step was at –1.4 V for 240 s. In the case of H_2O_2 assay the calibration plot was also constructed in the same e-well by nine successive additions of 1 µL of 150 mmol L^{-1} H_2O_2 in 100 µL PBS 0.1 mol L^{-1} (pH 7.0). The applied potential was –0.7 V. All potentials were reported with respect to the 3D printed carbon-PLA reference electrode.

For the CRP immunoassay, 150 µL per e-well of a 2.5 µg mL^{-1} goat polyclonal anti-CRP antibody solution in 50 mmol L^{-1} carbonate buffer (pH 9.2) were coated in 3D e-wells overnight. Next, the e-wells were rinsed twice with 300 µL of 50 mmol L^{-1} PBS (pH 7.4) containing 1% w/v BSA (washing buffer), and blocked with 300 µL of 10% v/v skimmed cow milk in 50 mmol L^{-1} PBS (pH 7.4) for 1 h. Then, the e-wells were washed twice as previously. For the assay, 150 µL of a 1:1 mixture containing CRP calibrators and 2.5 µg mL^{-1} biotinylated monoclonal anti-CRP antibody were added in the 3D e-wells and incubated for 45 min, under shaking. Then, the wells were washed four times with 300 µL washing buffer and reacted with 150 µL of STV–CdSe/ZnS QDs solution of 5 nmol L^{-1} QDs in PBS (50 mmol L^{-1}, pH 7.4, containing 1% w/v BSA) for 15 min. Then, the e-wells were washed four times with washing buffer and dried. Finally, 150 µL of a solution containing HNO_3 0.01 mol L^{-1} and 0.2 mg L^{-1} Bi(III) were added in each e-well and sonication was applied for 5 min to release Cd(II) from the core of QDs. Released Cd(II) was preconcentrated on the surface of Bi-film WE of 3D e-well at –1.4 V for 240 s, under shaking. Then, the potential of the WE was scanned from –1.1 to –0.3 V in the SW mode (frequency: 50 Hz; pulse height: 40 mV; step increment: 4 mV) and the signal was recorded.

Acknowledgements

This research was co-financed by Greece and the European Union (European Social Fund- ESF) through the Operational Program «Human Resources Development, Education and Lifelong Learning 2014–2020» in the context of the project "Three dimensional printed microdevices for electrochemical bioassays using quantum dots as labels" (MIS 5047951).

Conflict of Interest

The authors declare no conflict of interest.

Data Availability Statement

Research data are not shared.

Keywords

3D-printing, biosensors, electrochemistry, microwells, quantum dots

Received: March 12, 2021
Revised: March 24, 2021
Published online: April 20, 2021

[1] A. Gowri, N. Ashwin Kumar, B. S. Suresh Anand, *TrAC, Trends Anal. Chem.* **2021**, *137*, 116205.
[2] C. Wang, M. Liu, Z. Wang, S. Li, Y. Deng, N. He, *Nano Today* **2021**, *37*, 101092.
[3] A. Yang, F. Yan, *ACS Appl. Electron. Mater.* **2021**, *3*, 53.
[4] C. Kokkinos, A. Economou, M. I. Prodromidis, *TrAC, Trends Anal. Chem.* **2016**, *79*, 88.
[5] C. Kokkinos, *Nanomaterials* **2019**, *9*, 1361.
[6] E. J. Carrasco-Correa, E. F. Simó-Alfonso, J. M. Herrero-Martínez, M. Miró, *TrAC, Trends Anal. Chem.* **2021**, *136*, 116177.
[7] M. Elbadawi, J. J. Ong, T. D. Pollard, S. Gaisford, A. W. Basit, *Adv. Funct. Mater.* **2020**, *31*, 2006407.
[8] C. Kokkinos, A. Economou, *Curr. Opin. Electrochem.* **2020**, *23*, 21.
[9] Y. T. Seo, S. Jeong, J. K. Lee, H. S. Choi, J. Kim, H. Y. Lee, *Nano Convergence* **2018**, *5*, 9.
[10] N. B. Mincu, V. Lazar, D. Stan, C. M. Mihailescu, R. Iosub, A. L. Mateescu, *Diagnostics* **2020**, *10*, 517.
[11] P. Yáñez-Sedeño, S. Campuzano, J. M. Pingarrón, *Biosensors* **2020**, *10*, 76.
[12] C. L. Manzanares Palenzuela, M. Pumera, *TrAC, Trends Anal. Chem.* **2018**, *103*, 110.
[13] A. Abdalla, B. A. Patel, *Curr. Opin. Electrochem.* **2020**, *20*, 78.
[14] M. Sharafeldin, A. Jones, J. F. Rusling, *Micromachines* **2018**, *9*, 394.
[15] R. G. Rocha, R. M. Cardoso, P. J. Zambiazi, S. V. F. Castro, T. V. B. Ferraz, G. de O. Aparecido, J. A. Bonacin, R. A. A. Munoz, E. M. Richter, *Anal. Chim. Acta* **2020**, *1132*, 1.
[16] C. Kalinke, N. V. Neumsteir, P. Roberto de Oliveira, B. C. Janegitz, J. A. Bonacin, *Anal. Chim. Acta* **2021**, *1142*, 135.
[17] J. Giorgini Escobar, E. Vaněčková, Š. N. Lachmanová, F. Vivaldi, J. Heyda, J. Kubišta, V. Shestivska, P. Španěl, K. Schwarzová-Pecková, J. Rathouský, T. Sebechlebská, V. Kolivoška, *Electrochim. Acta* **2020**, *360*, 136984.
[18] M. A. B. Helú, L. Liu, *Electrochim. Acta* **2021**, *365*, 137279.
[19] F. M. Rabboh, G. D. O'Neil, *Anal. Chem.* **2020**, *92*, 14999.
[20] D. Livas, M. Trachioti, S. Banou, M. Angelopoulou, A. Economou, M. Prodromidis, P. Petrou, S. Kakabakos, C. Kokkinos, *Sens. Actuators, B* **2021**, *334*, 129614.
[21] E. Vlachou, A. Margariti, G. S. Papaefstathiou, C. Kokkinos, *Sensors* **2020**, *20*, 4442.
[22] C. Kokkinos, A. Economou, A. Pournara, M. Manos, I. Spanopoulos, M. Kanatzidis, T. Tziotzi, V. Petkov, A. Margariti, P. Oikonomopoulos, G. S. Papaefstathiou, *Sens. Actuators, B* **2020**, *321*, 128508.
[23] V. Katseli, A. Economou, C. Kokkinos, *Anal. Chem.* **2021**, *93*, 3331.
[24] R. M. Cardoso, P. R. L. Silva, A. P. Lima, D. P. Rocha, T. C. Oliveira, T. M. do Prado, E. L. Fava, O. Fatibello-Filho, E. M. Richter, R. A. A. Muñoz, *Sens. Actuators, B* **2020**, *307*, 127621.
[25] J. Muñoz, E. Redondo, M. Pumera, *Adv. Funct. Mater.* **2021**, 2010608.
[26] A. M. López Marzo, C. C. Mayorga-Martinez, M. Pumera, *Biosens. Bioelectron.* **2020**, *151*, 111980.
[27] V. A. O. P. Silva, W. S. Fernandes-Junior, D. P. Rocha, J. S. Stefano, R. A. A. Munoz, J. A. Bonacin, B. C. Janegitz, *Biosens. Bioelectron.* **2020**, *170*, 112684.
[28] G. Martins, J. L. Gogola, L. H. Budni, B. C. Janegitz, L. H. Marcolino-Junior, M. F. Bergamini, *Anal. Chim. Acta* **2021**, *1147*, 30.
[29] M. A. Farzin, H. Abdoos, *Talanta* **2021**, *224*, 121828.
[30] E. Valera, A. Hernández-Albors, M. P. Marco, *TrAC, Trends Anal. Chem.* **2016**, *79*, 9.
[31] C. Kokkinos, M. Prodromidis, A. Economou, P. Petrou, S. Kakabakos, *Anal. Chim. Acta* **2015**, *886*, 29.
[32] S. H. D. Ribeiro, L. M. Alves, J. M. R. Flauzino, A. C. R. Moço, M. S. Segatto, J. P. Silva, L. F. A. Borges, J. M. Madurro, A. G. B. Madurro, *Electroanalysis* **2020**, *32*, 2316.
[33] L. O. Resende, A. C. H. de Castro, A. O. Andrade, J. M. Madurro, A. G. Brito-Madurro, *J. Solid State Electrochem.* **2018**, *22*, 1365.
[34] A. M. V. Mohan, V. Rajendran, R. K. Mishra, M. Jayaraman, *TrAC, Trends Anal. Chem.* **2020**, *131*, 116024.

[35] V. Jovanovski, S. B. Hočevar, B. Ogorevc, *Curr. Opin. Electrochem.* **2017**, *3*, 114.
[36] N. Serrano, J. M. Díaz-Cruz, C. Ariño, M. Esteban, *TrAC, Trends Anal. Chem.* **2016**, *77*, 203.
[37] J. Ju, W. Chen, *Anal. Chem.* **2015**, *87*, 1903.
[38] M. Ş. Teker, E. Karaca, N. Ö. Pekmez, U. Tamer, K. Pekmez, *Electroanalysis* **2019**, *31*, 75.
[39] S. Karakaya, Y. Dilgin, *Anal. Lett.* **2019**, *52*, 998.
[40] G. Palla, K. Malecka, W. Dehaen, J. Radecki, H. Radecka, *Bioelectrochemistry* **2021**, *137*, 107643.